Respiratory Motion Compensation with Tracked Internal and External Sensors during CT Guided Procedures

J. Borgert[a,*], S. Krüger[a], H. Timinger[a], J. Krücker[b], N. Glossop[c], A. Durrani[d], B. J. Wood[d]

[a]*Philips Research Laboratories, Sector Technical Systems, Hamburg, Germany*
[b]*Philips Research USA, Briarcliff Manor, NY, USA*
[c]*Traxtal, Inc., Bellaire, TX, USA*
[d]*Diagnostic Radiology Department, National Institutes of Health, Bethesda, MD, USA*

Abstract. Position data from two electromagnetically tracked sensors, one placed on the patient's sternum, the other incorporated into a biopsy needle, were acquired during a liver biopsy. The data were used to evaluate the correlation between the position measurements of the two sensors and to derive an affine motion model to assess the possibility of using an external sensor for respiratory motion compensation for image-guided interventional procedures.

Keywords: Respiratory Motion Compensation; Interventional Navigation; Electromagnetic Tracking

1. Introduction

Recent studies [1-5] propose the use of electromagnetic tracking systems for image-guided interventions. During these procedures, the position of interventional devices such as needles, guidewires, and catheters is measured and displayed in relation to pre-procedural anatomical images. In contrast to well-established optical position measurement systems, electromagnetic tracking systems do not suffer from line-of-sight restrictions and are, therefore, especially suited for percutaneous procedures like abdominal biopsies and ablations.

A major limitation for accurate navigation during image-guided minimally invasive procedures has been accurate characterization and thus compensation of respiratory motion. Successful compensation should improve registration to the pre-procedural images to enable navigation in the presence of patient motion due to breathing.

This paper investigates the possibility of using an externally placed electromagnetic sensor in combination with a motion model to compensate for respiratory motion. An additional sternum-mounted sensor was tested clinically as a method of motion acquisition during an electromagnetically tracked biopsy. The data were analysed with respect to the correlation of the motion of the external and internal tracked device and to

* Corresponding author. *E-mail address*: joern.borgert@philips.com.

assess the possibility of deploying a motion model to compensate for the motion of the internal device due to respiration.

2. Materials and Methods

The raw data for the study were acquired during a tracked biopsy of a 15mm hepatocellular carcinoma, only briefly seen on early phase CT imaging. The biopsy was performed on a sedated, unventilated 61-year-old male patient. The respiratory cycle length varied between 3s and 5.5s, depending on the patient's state of sedation. Further studies are underway for internal tracking of biopsy and ablation.

Trackable needles with 5 degrees of freedom (DoF) with internal sensor coils embedded in the stylet tip were designed, tested, sterilized, and used for the procedure. An additional 6 DoF sensor was placed on the sternum. The needles were connected to an electromagnetic tracking system (NDI Aurora, Northern Digital Inc., Ontario, Canada), which was integrated into a custom-made tracking and visualization workstation prototype for interventional navigation. The system was used to acquire and log the position and orientation of the connected devices. For the current analysis, only position data were evaluated.

Data acquisition was performed with a mean rate of 32.5 samples per second for selected parts of the whole intervention, totalling 720 seconds of tracking data. During parts of this acquisition, the needle was advanced and repositioned in the liver. Two ranges of data with steady respiration, consecutively named data1 and data2, were selected for a detailed analysis and assessment of the motion model. One of the ranges included a needle manipulation, see Figures 1 and 2, to assess the interplay between this movement and the motion model. See Tab. 1 for characteristics of the data.

Table 1
Characteristics of the selected ranges of data with steady respiration.

	Duration	Number of samples	Number of respiratory cycles
data1	~34 seconds	1100	~9
data2	~46 seconds	1500	~10
	needle manipulation between 24.5 seconds and 30.5 seconds in data2		

The correlation of the motion of the needle placed in the liver with the sternum sensor was determined by correlation matrix analysis. The entries of the correlation matrix cor_{mn} are defined by the ratio of the entries of the covariance matrix cov_{mn} and the respective product of the standard deviations σ_m and σ_n,

$$cor_{mn} = \frac{cov_{mn}}{\sigma_m \sigma_n} = \frac{\langle (m - \langle m \rangle)(n - \langle n \rangle) \rangle}{\sigma_m \sigma_n}$$

with m and n running over all individual coordinates, i.e. $m, n \in \{x, y, z, x', y', z'\}$, and the square brackets denoting the mean over the set of samples under examination, for example $\langle x \rangle = \frac{1}{N} \sum_{i=1}^{N} x_i$ for $m = x$ and a total of N samples. Specific entries of the resulting 6x6 correlation matrix from all 6 coordinates provide information on the correlation between the coordinates of an individual sensor, which can be used to

identify predominant motion patterns, as well as on the correlation between coordinates from the two different sensors.

The sum over the absolute values of the entries of the submatrix for the correlation of the two different sensors is used as a measure to quantify their correlation. The individual entries range from –1 for complete anti-correlation to +1 for complete correlation, whereas a value of 0 represents no correlation at all. For a 3x3 matrix, the maximum measure is 9, so the percent correlation is given by $100\% \cdot (\sum |cor_{mn}|) / 9$.

The determination of the correlation was performed using a sliding window containing 150 samples, covering about 4.6 seconds of data, to determine the integral correlation for about 1 – 1.5 respiratory cycles, see Fig. 1. The mean and standard deviation of the correlation values in the sliding window were computed. This correlation analysis was performed for all of the available data, as well as for the selected ranges of steady respiration, data1 and data2.

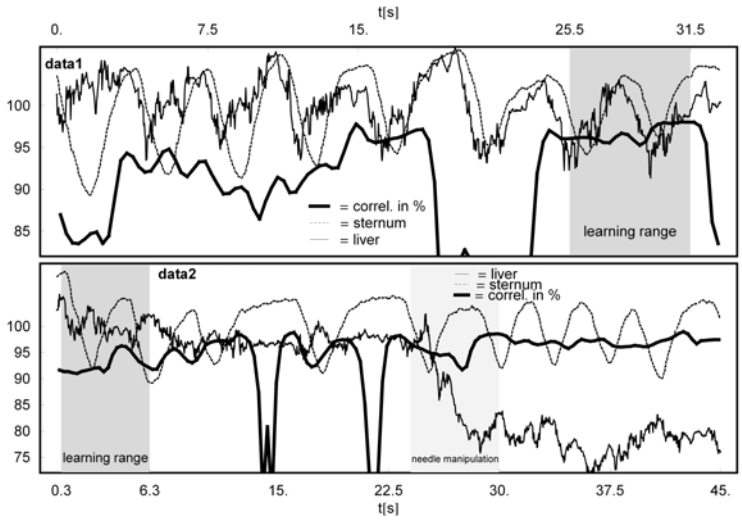

Figure 1. Absolute position of liver (thin solid) and sternum (thin dashed) sensor together with correlation for data1 (top) and data2 (bottom). Liver and sternum sensor positions are displayed in arbitrary scaling, whereas correlation is displayed as percentage.

To obtain a first impression of the potential of compensating the displacement of the internal sensor due to respiration, an affine motion model was derived using the parts of data exhibiting steady respiration (data1 and data2). When the needle is not advanced or retracted, the coordinates obtained from the position measurements should be constant, and any residual displacement is due to respiration assuming no needle slippage. The position measurements from the sternum sensor (the respiratory phase) and the related measurements from the liver sensor from a limited amount of data (marked learning range in Fig. 1) were used to derive a model for respiratory motion compensation. Applying the model to the data to be compensated, the residual displacement compared to the displacement without compensation is a measure of the effectiveness of the motion model.

To compensate an acquired position measurement of the liver sensor, its displacement from a given reference position due to respiratory motion is corrected by the respective displacement measured by the sternum sensor. Therefore, the displacement of the sternum sensor is transformed by an affine transformation to derive the appropriate correction for the liver sensor. The actual affine matrix A representing the transformation of the displacement of the sternum sensor to the displacement of the liver sensor is determined by minimizing

$$\sum \left(A \bullet \left(x_{disp.}^{sternum}, y_{disp.}^{sternum}, z_{disp.}^{sternum}, 1 \right) - \left(x_{disp.}^{liver}, y_{disp.}^{liver}, z_{disp.}^{liver}, 1 \right) \right)^2 .$$

The sum is running over all samples from the selected learning range, as depicted in Fig. 1. In this particular case, the reference position was chosen to be the mean position of the liver sensor over time. This ensures independence from any choice of reference and registration and is sufficient to measure the efficiency of the compensation. More realistically, the compensation would be referenced to the respiratory phase during image acquisition, which enables the relation of the liver sensors position to previously acquired image data. However, no respiratory phase information was acquired for this study.

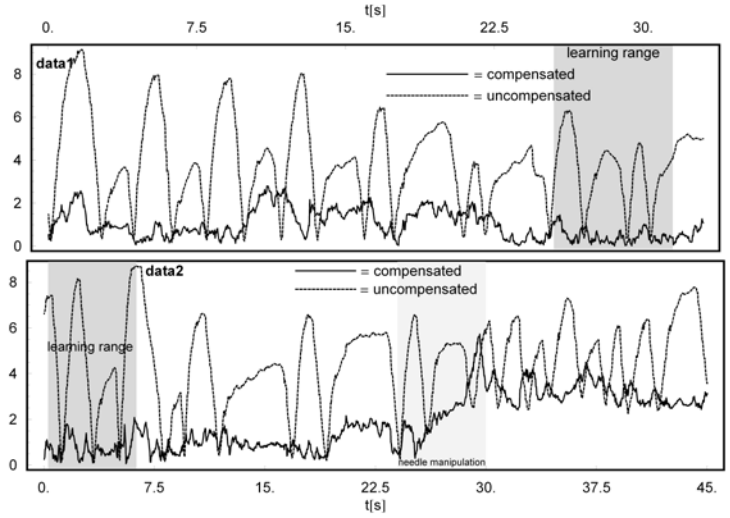

Figure 2. Uncompensated (dashed) and compensated (solid) residual displacement in mm for the needle placed in the liver for data1 (top) and data2 (bottom).

To measure the efficiency of the compensation, the affine model built from a subset of 200 samples (learning range, ~6 seconds) of data1 and data2 as shown in Fig. 1 was used to compensate all of the samples data1 and data2. In the data2 case, the evaluation of the efficiency of the compensation was performed for the first 23 seconds and the last 15 seconds separately, to assess how the compensation interplays with needle manipulations. The efficiency is given by a mean residual displacement after compensation together with a standard deviation.

3. Results

The overall distance between the liver sensor (intra-corporal) and the sternum sensor was 196.5mm ± 9.1mm during data acquisition.

The correlation between the motion of the sensor of the needle placed in the suspected carcinoma and the motion of the sensor on the sternum was 77.51% ± 19.44% for all available data (720 seconds). The correlation for the selected ranges of steady respiration showed a value of 90.54% ± 7.80% for data1 and 94.61% ± 5.63% for data2. Fig. 1 is showing the absolute values of the respective position measurements (in arbitrary scaling) together with the sliding window correlation in percent for data1 and data2.

Table 2
Residual displacement after affine motion compensation. Data for free form model for comparison.

Learned from	Applied to	Residual displacement	Min/max range
~6 sec. of data1	all of data1	0.99mm ± 0.66mm	0.02—2.79
	(free form model	1.04mm ± 0.91mm)	
~6 sec. of data2	first 23 seconds of data2	0.94mm ± 0.46mm	0.08—2.16
	last 15 seconds of data2	3.18mm ± 0.48mm	2.42—4.49
	(free form model (all of data2)	1.99mm ± 1.09mm)	
displacement of data1 without compensation		3.90mm ± 2.00mm	0.24—9.14
displacement of data2 without compensation		4.18mm ± 2.10mm	0.11—8.71

Without motion compensation, the mean residual displacement from the mean position of the liver sensor amounts to 3.90mm ± 2.00mm for data1 and 4.18mm ± 2.10mm for data2. After compensation, an improvement of the residual displacement to 0.99mm ± 0.66mm for data 1 (~factor 4) and 0.94mm ± 0.46mm for the first 23 seconds of data2 (also ~factor 4) could be realized. The last 15 seconds of data2 resulted in a residual displacement of 3.18mm ± 0.48mm, which clearly reflected the needle's movement, which amounted to approximately 3mm. Subtracting this extra displacement from the residual displacement leads to comparable results as in the case without manipulation. Fig. 2, bottom, is showing the influence of the needle manipulation on the compensation and the residual displacement, which clearly reflects the needle's movement. The reduction in standard deviation from the uncompensated case to the compensated case amounts to an improvement by a factor of ~4 in all cases, including the case after needle manipulation.

The results for the compensation of data1 and data2 can be compared to a compensation using a free form deformation model as described in [6,7] using radial basis functions [8] for interpolation. This compensation resulted in a residual displacement of 1.04mm ± 0.91mm for data1 and 1.99mm ± 1.09mm for data2.

Applying a dynamic affine motion model and an adaptive formulation of the affine transformation used for correcting the displacement of the liver sensor showed an even better performance as the static case presented here. As a drawback, this model had problems with the quantification of the needle's movement, which should be overcome by a more sophisticated formulation of the approach.

4. Conclusions

An affine respiratory motion model was developed to make use of external electromagnetic sternum tracking during CT guided interventions. It was demonstrated that the motion of an additional, electromagnetically tracked sensor placed on the patient's sternum shows a high correlation with a sensor introduced into an inner organ. The overall correlation without pre-selection of data is already high (nearly 78%), although it contains all types of motion artifacts including, for example, advancing or repositioning the needle as well as overall patient motion causing organ shift.

For the ranges of steady respiration without or with only minimal needle or patient motion, the correlation reaches up to 94% for several respiratory cycles (about 10).

An affine motion model driven by the motion data of the sternum sensor reduced the residual displacement of the internal sensor by a factor of approximately 4. It was furthermore possible to qualitatively and quantitatively detect the manipulation of the needle between 24.5 seconds and 30.5 seconds in data2.

Given the high correlation, it can be expected that the combination of internally tracked sensors with additional external sensors on the patient's sternum can be used as a reliable means for respiratory motion detection and compensation. The general applicability of this finding will have to be proven in further studies, together with the assessment of more sophisticated models for motion compensation. Such models could include elastic deformable dynamic models to account for tissue warping, as may occur with applied torque during needle manipulations.

The potential correction of respiratory misregistration with a compensation model will play an important role in successful integration and clinical application of electromagnetic tracking of medical devices.

References

[1] B.J. Wood, H. Zhang, A. Durrani, N. Glossop, S. Ranjan, D. Lindisch, E. Levy, F. Banovac, J. Borgert, S. Krüger, J. Krücker, A. Viswanathan, K. Cleary. Navigation with Electromagnetic Tracking for Interventional Radiology Procedures: A Feasibility Study, *Journal of Vascular and Interventional Radiology,* in press, 2005

[2] S.B. Solomon, T. Dickfield, H. Calkins. Real-time cardiac catheter navigation on three-dimensional CT images. Journal of Interventional Cardiac Electrophysiology, 8:27-36, 2003

[3] S.B. Solomon, P. White, C.M. Wiener, J.B. Orens, K.P. Wang. Three-dimensional CT-guided bronchoscopy with a real-time electromagnetic position sensor, Chest, 118:1783-1787, 2000

[4] S.B. Solomon, C.A. Magee, D.E. Acker, A.C. Venbrux. Experimental nonfluoroscopic placement of inferior vena cava filters: Use of an electromagnetic navigation system with previous CT data, *Journal of Vascular and Interventional Radiology, 10:92-95, 1999*

[5] S.A. Ben-Haim, D. Osadchy, I. Schuster, L. Gepstein, G. Hayam, and M.E. Josephson. Nonfluoroscopic, in vivo navigation and mapping technology, *Nature Medicine*, 2(12), pp. 1393-1395, 1996

[6] H. Timinger, S. Krüger, K. Dietmayer, and J. Borgert. Motion compensation for interventional navigation on 3D static roadmaps based on a dynamic motion model. *Proceedings of Computer Assisted Radiology and Surgery (CARS), International Congress Series, Elsevier,* 1268:1055-1060, 2004

[7] H. Timinger, S. Krüger, K. Dietmayer, and J. Borgert. Motion compensated coronary interventional navigation by means of diaphragm tracking and elastic motion models. *Physics in Medicine and Biology.* 50(3):491-503, 2005

[8] R.L. Hardy. Multiple equations of topography and other irregular surfaces. *Journal of Geophysical Research,* 76(8):1905-1915, 1971